

09,12,04

Thermostimulated luminescence mechanisms of UV irradiated zirconium dioxide nanotubes

© I.A. Petrenyov¹, A.S. Vokhmintsev¹, S.A. Starovoytova¹, I.A. Weinstein^{1,2}

¹ Ural Federal University after the first President of Russia B.N. Yeltsin, Yekaterinburg, Russia

² Institute of Metallurgy of Ural Branch of the Russian Academy of Science, Yekaterinburg, Russia

E-mail: i.a.petrenev@urfu.ru

Received July 8, 2021

Revised July 8, 2021

Accepted July 8, 2021

A nanotubular layer of zirconium dioxide was synthesized with anodic oxidation. Curves of spectrally resolved thermostimulated luminescence were studied in the 390–550 nm range after 300 nm UV irradiation. Energetic and kinetic parameters of thermostimulated luminescence curves were estimated. The mechanism of thermally-activated processes involving intrinsic lattice defects is proposed.

Keywords: Spectrally resolved thermostimulated luminescence, zirconium dioxide, nanotubes, electron and hole traps.

DOI: 10.21883/PSS.2022.13.52305.09s

1. Introduction

Nanopore and nanotubular massives of the Zirconium dioxide (ZrO₂-nt) are used in various areas of science and engineering, thanks to a high chemical, mechanical and temperature stability and the surface area [1–3]. They are used as the basis for manufacture of batteries, condensers, fuel elements, solid electrolytes, catalysts, dose meters and memristors [4–7].

It is known, that point defects (F⁻, F⁺- and Zr³⁺-centers) and their aggregates (e.g., T-defects [8], vacancies clusters [9], etc.) are optically active centers that form peculiarities of the Zirconium dioxide response to various external effects. Earlier, the nanotubes ZrO₂-nt made by anodic treatment, were studied by using spectral methodologies of photoluminescence (PL) [10–17] and galvanoluminescence [18]. In addition, a series of works referred to the methods of thermally-stimulated luminescence (TSL) within the spectral range 400–650 nm for the study of monoclinic ZrO₂ powders in the original state and after high-temperature treatments in the air [7,9–24], in the vacuum [35] or in argon atmosphere [26]. Experimental confirmations were obtained as to the presence of the charge carrier traps that are active below the room temperature (223–293 K) [26] and within a wide temperature range from 300 to 750 K [7,19–25] after exposure of samples to electron beam [7,19,25], β - [20–23] or UV-radiation [24,26]. The studies of nanotubular structures of the Zirconium dioxide by TSL method are unknown as for now.

Therefore, the purpose of this work was to study the thermal activating processes in the synthetic massives of nanotubes ZrO₂ after exposure to UV-radiation.

2. Samples and methods

Nanotubular massives of the Zirconium dioxide ZrO₂-nt was synthetically produced by anode treatment of Zr-foil with the admixture of Hf < 1% [27]. Zr-foil with the thickness of 100 μ m was preliminarily degreased, submerged into ultrasonic bath, treated by solution of acids HF:HNO₃:H₂O = 1:6:20, washed with distilled water and dried on the air. Anode treatment was done in two-electrode electrochemical cell at constant voltage of 20 V and the anode temperature 10°C during 6 hr.

Electrolyte was a solution of ethylene glycol containing 5 wt.% H₂O and 1 wt.% NH₄F.

The morphological parameters of synthetically produced layers were studied by means of scanning electron microscope (SEM) SIGMA VP made by Carl Zeiss. On the SEM image given in Fig. 1 one can see the oxide layer consisting of self-ordered nanotubes with the diameter of 50 nm. In case of anode oxidation of Zr-foil under the abovementioned conditions the thickness of the synthetically produced massifs ZrO₂-nt makes $\sim 5 \mu$ m [27].

After the synthesis the layers of ZrO₂-nt were heated up to 800 K in the air in order to remove residues of electrolyte. The samples for TSL studies represented a rectangular Zr-substrate with the size of 12 \times 7 mm with the layer of ZrO₂-nt on one side of the metal.

TSL curves measurement was performed at luminescent spectrometer Perkin Elmer LS 55 with high-temperature add-on [28]. TSL studies were performed within the range of temperatures $T = 300$ –773 K at the heating rate

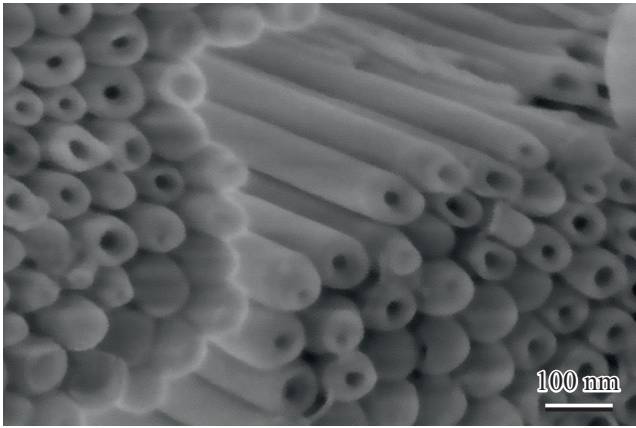


Figure 1. Image of synthetically produced nanotubes ZrO₂-nt.

$\beta = 2$ K/s. Prior to TSL measurement the samples were heated to 773 K for emptying the traps, and cooled down to the room temperature inside the obscured spectrometer chamber. Thereafter the studied samples were subjected to impact of monochromic UV-radiation with the wave length $\lambda = 300$ nm (4.1 eV) during 10 min. at the room temperature. The UV-dose was 1 mJ/cm². Spectrum-resolved TSL was measured within the range of the wave lengths from 390 to 550 nm with the pitch of 20 nm, slot in the recorder monochromator was 20 nm.

Experimental curves of TSL were analyzed within the framework of formalities of the kinetics of total order [29]:

$$I(T) = s'' n_0 \exp\left(-\frac{E_a}{kT}\right) \times \left[1 + \frac{s''(b-1)}{\beta} \int_{T_0}^T \exp\left(-\frac{E_a}{kT'}\right) dT'\right]^{\frac{b}{b-1}}, \quad (1)$$

where $I(T)$ — intensity of TSL; s'' — efficient frequency factor, s⁻¹; n_0 — initial concentration of filled traps after exposure, m⁻³; E_a — energy of thermal ionization, eV; k — Boltzmann’s constant, eV/K; T — temperature, K; b — kinetics order; β — heating rate, K/s; $T_0 = 300$ K — initial temperature, K.

Energetic and kinetic characteristics of the entrapment centers were determined by approximation of the TSL curves shape by superposition of several independent peaks of the total order kinetics according to exp. (1). This methodology is successfully applied in TSL of dosimetry of ionizing radiation during the study of wide-bandgap materials [20–23,30,31].

3. Results and discussion

3.1. TSL curves in different luminance bands

Fig. 2 shows TSL curves measured in the studied luminance bands. It can be seen that all thermoactivation

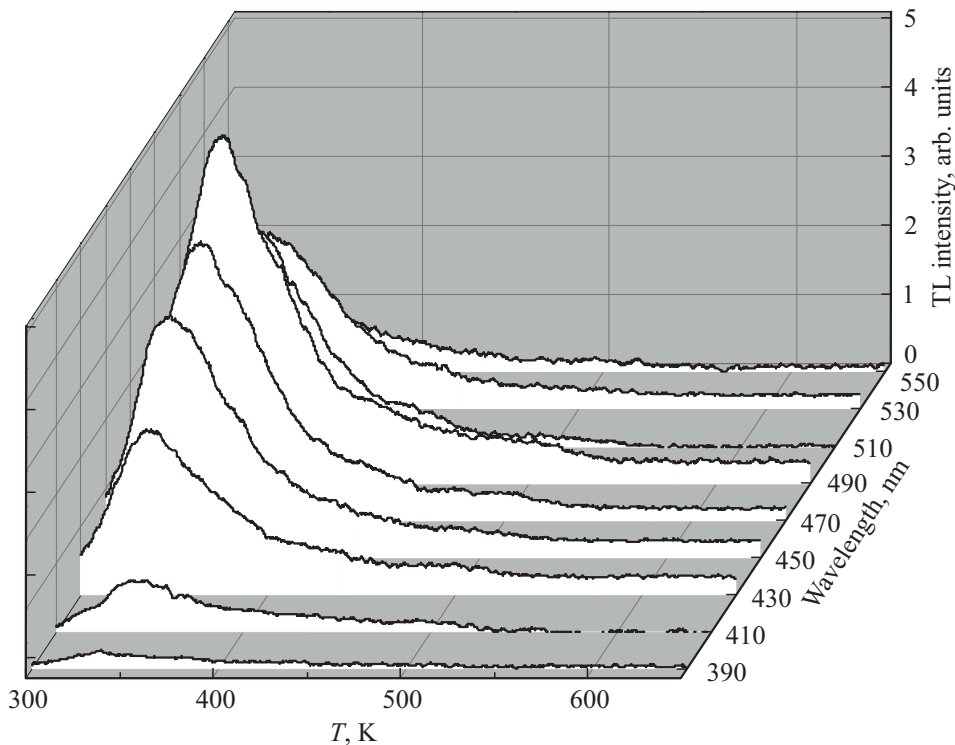


Figure 2. Experimental TSL curves at various recording wave lengths.

curves have one peak with the maximum at the temperature about 340 K, and in the interval of 400–550 K a less intensive shoulder is recorded for each of them. Note, that all experimental curves in the studied spectral interval have similar shape and that the highest intensity of TSL is observed within the band 490 nm. Then, for interpretation of the nature of recombination centers participating in the recorded thermoactivation processes within the studied temperature range, we built and analyzed the TSL luminance spectrum.

3.2. Spectral characteristics of TSL

Fig. 3 shows dependence of the TSL light sum on the energy of photons for $\text{ZrO}_2\text{-nt}$. Every point of the spectrum corresponds to the area under experimental TSL-curve (Fig. 2) within the mentioned temperature range for the studied luminance bands.

It can be seen that TSL spectrum is satisfactorily described by two peaks of Gaussian shape G1 and G2 with the energies of the maximum $E_{\text{max}} = 2.47 \pm 0.02$ and 2.72 ± 0.03 eV and half-width $\omega = 0.23 \pm 0.04$ and 0.39 ± 0.12 eV, accordingly. The obtained results coincide with our studies of PL properties of nanotubular layers ZrO_2 [10], for which also two luminance bands are recorded with the Gaussian shape $E_{\text{max}} = 2.43 \pm 0.01$ and 2.68 ± 0.03 eV, as well as $\omega = 0.35 \pm 0.01$ and 0.48 ± 0.02 eV, accordingly. Moreover, in independent studies of the samples of powders of monoclinical ZrO_2 in the TSL spectra [7,19–26], PL [7,23,25,26] and impulse cathode luminescence [7,25] a wide non-elementary luminance band is recorded within the range 400–650 nm (3.10–1.91 eV) with the maximum in the interval 480–500 nm (2.58–2.48 eV).

Therefore, close spectral composition of luminescence at different types of excitation $\text{ZrO}_2\text{-nt}$ and powders of monoclinical ZrO_2 may indicate predominance of monoclinical phase in the studied samples. The mentioned fact also coincides the studies of nanotubes $\text{ZrO}_2\text{-nt}$ by using the method of X-ray diffraction, for which formation of monoclinical phase is recorded as a result of annealing at 400°C during 1 hr in the air [32]. At the same time one may conclude on participation of two centers of the irradiation recombination in the studied thermoactivation processes.

Analysis of publications has shown, that luminance within the band G1 (~ 2.4 eV) is related with recombination of holes from the valence band with electrons entrapped by ions of Zr^{3+} [8]. As for today, there is no definitive opinion on the nature of the band G2 (2.5–2.7 eV) [25]. Someone associate the luminescence with relaxation of admixed ions Ti^{3+} , which can be available in ZrO_2 in very low concentrations [33]. In our case the presence of admixed ions Ti in the studied samples is excluded at the synthesis stage. Someone other — associate it with relaxation of oxygen vacancies within the volume or on the surface of the sample [34,35]. There are also opinions on participation of complex defects that include

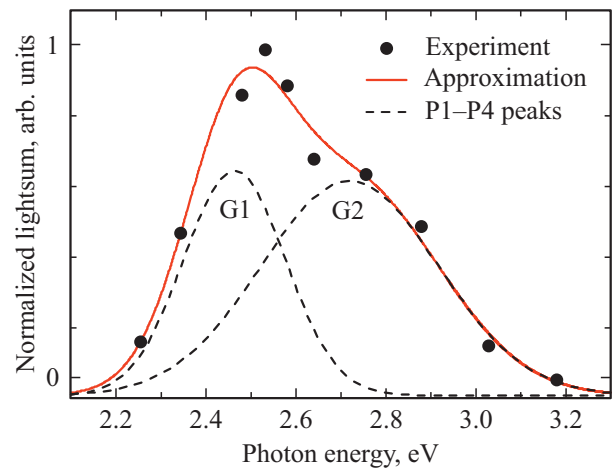


Figure 3. Breakdown of the TSL spectrum into Gaussian peaks.

associated oxygen vacancies [36] or ions Zr^{3+} , related with two neighboring oxygen vacancies (T-centers) [8].

Possible participation of T-centers in the mechanisms of recorded TSL satisfactorily correlates with the position of the level of excited state of T-defects, which is located 4.2 eV above the top of the valence band [8]. Note, that the applied method of synthesis of the samples $\text{ZrO}_2\text{-nt}$ and their developed surface contributes into accumulation of a high number of oxygen vacancies and ions Zr^{3+} , accordingly. At the same time the probability of formation of T-centers is increased, which is confirmed by comparable intensities of Gaussian components in the TSL spectrum (Fig. 3).

3.3. Assessments of energetic and kinetic parameters

Fig. 4 shows approximations of experimental TSL curves in the bands $\lambda_{\text{em}} = 490$ and 430 nm, related to luminance in the bands G1 and G2, accordingly. Breakdowns were done by using superposition of 4 peaks (P1–P4) of the total order of kinetics according to exp. (1). Table presents the obtained values of approximation parameters with coefficients of determination $R^2 > 0.999$.

Analysis of Table has shown, that the values T_{max} for TSL peaks in the band $\lambda_{\text{em}} = 430$ nm are shifted to the low-temperature band by 2–10 K relative to the values T_{max} of corresponding peaks in the band $\lambda_{\text{em}} = 490$ nm. In TSL mechanisms determining the peaks P1–P3, there is predominance of the processes of the second order of kinetics, and for the peaks P4 — of the first order. All observed peaks feature close values E_a . For the peaks P1 and P2 the values of effective frequency factor vary within the range $s'' = (8.5\text{--}6.2) \cdot 10^9 \text{ s}^{-1}$, and for the peaks P3 and P4 — $s'' = (9.7\text{--}0.9) \cdot 10^7 \text{ s}^{-1}$. Therefore, similar nature of description of the TSL curves mean that the same charge carrier traps determine the studied TSL processes in the studied luminance bands.

The obtained values of parameters of the thermoactivation processes (Table) satisfactorily correlate with the TSL studies of the powder of monoclinic ZrO_2 within the band 350–450 nm after β -exposure to the dose of 10 Gy [22]. In this work, the TSL curves were described as four peaks of the first order of kinetics with close values $E_a = 0.69–0.74$ eV and $s = 3 \cdot 10^8–9 \cdot 10^9$ s⁻¹. The authors of the work [22] associated the TSL peaks with four electron traps.

Note, that in our case the values of the parameter s'' for the peaks P1 and P2 are hundredfold higher than similar values for the peaks P3 and P4 with close values $E_a = 0.71–0.80$ eV and change of the values T_{max} of peaks from 334 to 496 K. According to the data of the works [37,38], oxygen vacancies ZrO_2 are electron traps with $E_a \approx 0.7$ eV. At the same time, according to the analysis work [39] the intra-node ions O_i^{2-} surrounded by three Zr-ions, represent hole traps and have the hole affinity energy equal to 0.78 eV. This, in turn, also corresponds to the range of the obtained values E_a for the peaks P1–P4 (Table).

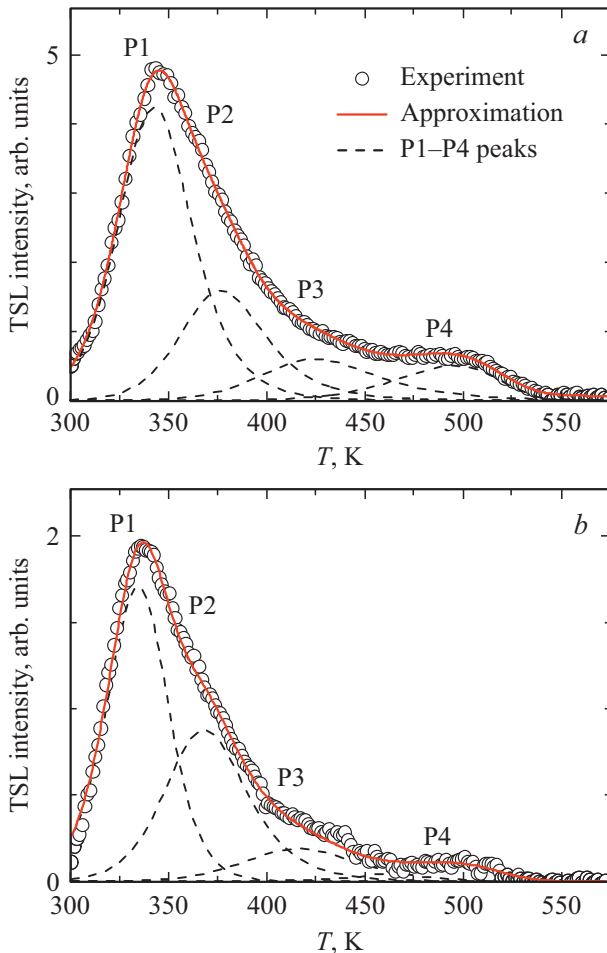


Figure 4. Breakdown of the TSL curve in the bands *a*) 490 and *b*) 430 nm into elementary components of the total order of kinetics.

Values of the temperature of the maximum T_{max} , ionization energy E_a , frequency factor s'' and order of kinetics b for the peaks P1–P4 in the bands 490 and 430 nm

Peak	λ_{em} , nm	T_{max} , ± 2 K	E_a , ± 0.03 eV	s'' , s ⁻¹	b
P1	490	343	0.73	$8.3 \cdot 10^9$	1.9
	430	334	0.76	$8.5 \cdot 10^9$	1.6
P2	490	377	0.80	$8.0 \cdot 10^9$	2.0
	430	367	0.78	$6.2 \cdot 10^9$	2.0
P3	490	425	0.76	$9.7 \cdot 10^7$	2.0
	430	416	0.71	$2.1 \cdot 10^7$	1.8
P4	490	496	0.80	$8.6 \cdot 10^6$	1.1
	430	494	0.80	$1.0 \cdot 10^7$	1.0

Therefore, found spectral peculiarities of TSL and obtained parameters of the entrapment centers (see Table), as well as their comparison to independent experimental and theoretical works [8,25,32–39] allow proposing a model of the mechanisms for the studied TSL processes in nanotubular massifs of Zirconium dioxide with participation of both electron, and hole traps.

In case of intra-band excitation of the samples ZrO_2 -nt by monochromatic UV-radiation with the energy of 4.1 eV the following TSL processes go on. With absorption of a photon with the energy of 4.1 eV e goes from the valence band to the excitation level of T-defect with further non-irradiating relaxation e to the level Zr^{3+} -center. At the same time, h generated in the valence band is entrapped by the intra-node ion O_i^{2-} . Next, in case of repeated absorption of a photon with the energy of 4.1 eV e goes to the conductivity band and is entrapped by oxygen vacancy (V_O). Then, heating of UV-irradiated samples results in appearance of free e and h in the conductivity and valence bands, accordingly. Further, irradiative recombination is recorded with participation of Zr^{3+} -centers (within the band G1), as well as F^- , F^+ -centers and their complexes (within the band G2).

4. Conclusion

Nanotubular layers of ZrO_2 -nt with the thickness of 5 μ m and internal diameters of nanotubes of 50 nm were synthetically produced by using the anode treatment method. A series of the TSL curves was measured in fixed luminance bands within the range of 390–550 nm of the samples ZrO_2 -nt after exposure to UV-radiation.

Two Gaussian components G1 and G2 with the maximums at 2.47 and 2.72 eV, accordingly, were found in the TSL luminance spectrum. Analysis of publications has shown, that luminance within the band G1 is related with recombination of holes from the valence band with electrons entrapped by ions of Zr^{3+} , and within the band G2 — with participation of F^- , F^+ -centers and their complexes.

Breakdown of TSL curves was made by superposition of four peaks of total order of kinetics. Energetic and kinetic characteristics of the recorded TSL processes were determined. Conclusions were made that electron traps are oxygen vacancies, and the hole traps — are intranode ions of oxygen with the values of energies of thermal ionization $E_a = 0.7-0.8$ eV. Based on the obtained data and performed analysis of publications the mechanisms are proposed for the observed thermoactivation processes in nanotubes ZrO₂ after exposure to UV-radiation.

Work funding

The work was done within the framework of research project FEUZ-2020-0059 of the Ministry of science and higher education of the Russian Federation.

Conflict of interest

The authors declare that they have no conflict of interest.

References

- [1] H. Tsuchiya, J.M. Macak, A. Glicov, L. Taveira, P. Schmuki. *Corros. Sci.* **47**, 12, 3324 (2005).
- [2] H. Tsuchiya, J.M. Macak, I. Sieber, P. Schmuki. *Small* **1**, 7, 722 (2005).
- [3] W.-J. Lee, W.H. Smyrl. *Electrochem. Solid-State Lett.* **8**, 3, B7 (2005).
- [4] D. Panda, T.-Y. Tseng. *Thin Solid Films* **531**, 1 (2013).
- [5] A.S. Vokhmintsev, R.V. Kamalov, A.V. Kozhevina, I.A. Petrenyov, N.A. Martemyanov, I.A. Weinstein. *Proceed. US-BEREIT* **2018**, 348 (2018).
- [6] I.A. Petrenyov, A.S. Vokhmintsev, R.V. Kamalov, I.A. Weinstein. *AIP Conf. Proceed.* **2174**, 020242 (2019).
- [7] S.V. Nikiforov, V.S. Kortov, M.G. Kazantseva, K.A. Petrovykh. *J. Lumin.* **166**, 111 (2015).
- [8] V.M. Orera, R.I. Merino, Y. Chen, R. Cases, P.J. Alonso. *Phys. Rev. B* **42**, 16, 9782 (1990).
- [9] D.S. Aidhy, Y. Zhang, W.J. Weber. *Scripta Mater.* **98**, 16 (2015).
- [10] A.S. Vokhmintsev, R.V. Kamalov, I.A. Petrenyov, I.A. Weinstein. *AIP Conf. Proceed.* **2313**, 030033 (2020).
- [11] F. Trivinho-Strixino, F.E.G. Guimarães, E.C. Pereira. *Chem. Phys. Lett.* **461**, 1–3, 82 (2008).
- [12] F. Trivinho-Strixino, F.E.G. Guimarães, E.C. Pereira. *Mol. Cryst. Liq. Cryst.* **485**, 766 (2008).
- [13] X. Wang, J. Zhao, P. Du, L. Guo, X. Xu, C. Tang. *Mater. Res. Bull.* **47**, 11, 3916 (2012).
- [14] M. Wang, X. Wang, J. Lin, X. Ning, X. Yang, X. Zhang, J. Zhao. *Ceram. Int.* **41**, 7, 8444 (2015).
- [15] N. Fu, X. Wang, L. Guo, J. Zhao, X. Zhang, J. Lin, L. Cong, M. Wang, Y. Yang. *J. Mater. Sci. Mater. Electron.* **28**, 10, 7253 (2017).
- [16] D. Liu, M. Wang, L. Gong, J. Zhao, M. Zhu, X. Wang. *J. Alloys Compd* **864**, 158781 (2021).
- [17] E.-Y. Seo, S.-K. Choi, I.-S. Shin, W.-K. Kang. *J. Kor. Chem. Soc.* **57**, 5, 547 (2013).
- [18] S. Stojadinović, R. Vasilčić, M. Petković, I. Belča, B. Kasalica, M. Perić, Lj. Zeković. *Electrochim. Acta* **79**, 133 (2012).
- [19] S.V. Nikiforov, V.S. Kortov, D.L. Savushkin, A.S. Vokhmintsev, I.A. Weinstein. *Radiation Measurements* **106**, 155 (2017).
- [20] H.S. Loksha, K.R. Nagabhushana, F. Singh. *J. Lumin.* **192**, 173 (2017).
- [21] H.S. Loksha, N. Chauman, K.R. Nagabhushana, F. Singh. *Ceram. Int.* **44**, 15, 18871 (2018).
- [22] H.S. Loksha, M.L. Chithambo, S. Chikwembani. *J. Lumin.* **218**, 116864 (2020).
- [23] H.S. Loksha, K.R. Nagabhushana, F. Singh. *Opt. Mater.* **107**, 109984 (2020).
- [24] Y. Cong, B. Li, B. Lei, W. Li. *J. Lumin.* **126**, 2, 822 (2007).
- [25] S.V. Nikiforov, A.A. Menshenina, S.F. Konev. *J. Lumin.* **212**, 219 (2019).
- [26] V. Kiisk, L. Puust, K. Utt, A. Maaros, H. Mändar, E. Viviani, F. Piccinelli, R. Saar, U. Joost, I. Sildos. *J. Lumin.* **174**, 49 (2016).
- [27] I.A. Petrenyov, R.V. Kamalov, A.S. Vokhmintsev, N.A. Martemyanov, I.A. Weinstein. *J. Phys. Conf. Ser.* **1124**, 2, 022004 (2018).
- [28] A.S. Vokhmintsev, M.G. Minin, A.M.A. Henaish, I.A. Weinstein. *Measurement* **66**, 90 (2015).
- [29] S.W.S. McKeever, R. Chen. *Radiation Measurements* **27**, 5–6, 625 (1997).
- [30] I.A. Weinstein, A.S. Vokhmintsev, M.G. Minin, V.V. Kartashov, I.V. Chernetsky. *Radiation Measurements* **56**, 236 (2013).
- [31] A.S. Vokhmintsev, M.G. Minin, I.A. Weinstein. *Radiation Measurements* **106**, 55 (2017).
- [32] A.V. Kozhevina, A.S. Vokhmintsev, R.V. Kamalov, N.A. Martemyanov, A.V. Chukin, I.A. Weinstein. *J. Phys. Conf. Series* **917**, 6, 062031 (2017).
- [33] Y. Cong, B. Li, S. Yue, D. Fan, X. Wang. *J. Phys. Chem. C* **113**, 31, 13974 (2009).
- [34] T.V. Perevalov, D.V. Gulyaev, V.S. Aliev, K.S. Zhuravlev, V.A. Gritsenko, A.P. Yelissejev. *J. Appl. Phys.* **116**, 24, 244109 (2014).
- [35] N.G. Petrik, D.P. Taylor, T.M. Orlando. *J. Appl. Phys.* **85**, 9, 6770 (1999).
- [36] N. Korsunskaya, V. Papusha, O. Kolomys, V. Strelchuk, A. Kuchuk, V. Kladko, Yu. Bacherikov, T. Konstantinova, L. Khomenkova. *Phys. Status Solidi C* **11**, 9–10, 1417 (2014).
- [37] C. Bettinali, G. Ferbaresso, J.W. Manconi. *J. Chem. Phys.* **50**, 9, 3957 (1969).
- [38] K.A. Shoaib, F.H. Hashmi, M. Ali, S.J.H. Bukhari, C.A. Majid. *Phys. Status Solidi* **40**, 2, 605 (1977).
- [39] A.S. Foster, V.B. Sulimov, F. Lopez Gejo, A.L. Shluger, R.M. Nieminen. *Phys. Rev. B* **64**, 22, 224108 (2001).